Article

Towards a Due Foundation for Image Based Discrimination of Multiple Sclerosis Disease Types Using Magnetic Levitation and Vision Intelligence

Milad Ramezankhani[1], Tina Olfatbakhsh[1], Ali Akbar Ashkarran[2], Dalia Abou Zeki[3], Irina Radu[3], Farnaz Khalighinejad[3], Kiandokht Keihanian[3], Carolina Ionete*[3], Abbas S. Milani[1], Morteza Mahmoudi[2]* and Sepideh Pakpour[1]*

[1]School of Engineering, University of British Columbia, Kelowna and V1V1V7 Canada
[2]Department of Radiology and Precision Health Program, Michigan State University, East Lansing, MI, USA
[3]Department of Neurology, University of Massachusetts, Worcester, MA, USA
[4]Department of Dermatology, University of Massachusetts, Worcester, MA, USA
* Correspondence: to: (CI) email: Carolina.Ionete@umassmemorial.org; (MM) email: mahmou22@msu.edu; (SP) email: sepideh.pakpour@ubc.ca

Abstract: The emerging advancements in separation and classification of various biological matters (e.g., living cells and proteins) using magnetic levitation (MagLev) technology have proven to be effective for improving disease diagnostics. MagLev technique has the capacity to detect and separate useful diagnostic biomarkers from biocomplex environments (e.g., blood and plasma), minimizing the unpleasant daunting task of sample preparations and labeling procedures. Here, we demonstrate the capability of this technique combined with image analysis and machine learning approaches for discriminating the various types of multiple sclerosis (MS) as an important model disease. To arrive at a systematic expert system, we combined robust statistical analysis with machine learning to (1) detect and remove outliers from the raw MagLev image datasets; then (2) process the images and output a low dimensional representation of massive data without losing the main statistical features; and finally (3) predict the MS clinical disease type (Relapsing-Remitting, Primary–Progressive, or Secondary–Progressive) using a classifier. This is expected to improve MS diagnostics since the current practices rely solely on clinical observation and central nervous system imaging, making management approaches are often reactional and inefficient. Thus, there is a need to identify the disease type early on. MagLev is expected to improve MS diagnostics, thereby aiding in prognosis and guiding adequate treatment choices before the patient exhibits signs of permanent neurological deficits.

Keywords: magnetic levitation; multiple sclerosis; diagnostics; robust machine learning; pattern recognition

1. Introduction

Multiple sclerosis (MS) disease is the most widespread chronic progressive neurological disorder affecting young patients in the world (Lublin, 2014; Wallin et al., 2019), with the mean age affected being 30 (Reich et al., 2018). It is estimated that 2.3 million people were affected by MS worldwide in 2019, and 1 million were living in the US (Nelson et al., 2019), more than twice the reported number in 1975. Its debilitating nature is related to multiple disease relapses and accumulated deficits over the patient's lifetime, leading some to be wheelchair-bound in the early years of adulthood. Research over the past few years helped shed light on the underlying pathology and resulted in 20 available agents for the treatment of MS disease (Hauser and Cree, 2020). Despite the advances, we still face ambiguity in early disease identification, management and selection of the best personalized treatment. Identifying biomarkers for diagnosis and prognosis has long been investigated at various stages of development. The clinicians, however, still rely on

Preprints (www.preprints.org) | NOT PEER-REVIEWED | Posted: 10 November 2022 doi:10.20944/preprints202211.0187.v1

clinical acumen in identifying neurological examination changes, monitoring for relapses or progression, performing a series of central nervous system (CNS) imaging, and adjusting the medications accordingly. The goal is to get to a stage where no disease activity is detectable, commonly referred to as "No Evidence of Disease Activity" (NEDA) (Alastair Compston Ian McDonald John Noseworthy Hans Lassmann David Miller Kenneth Smith Hartmut Wekerle Christian Confavreux, 2005; Axtell et al., 2010). While the common approach is either induction or escalation of therapy to delay progression, there is much room for interrater variability in practice resulting in missing the early time window of intervention and accumulation of irreversible damage and triggering slowly progressive CNS neurodegeneration. Various types of MS have been reported so far including relapsing-remitting MS (RRMS), secondary-progressive MS (SPMS), primary-progressive MS (PPMS) and progressive-relapsing MS (PRMS) (Axtell et al., 2010). For the final diagnosis of PPMS, the McDonald criteria require one year of observation and for secondary progressive the diagnostic may take years. There is a strong need for an early, fast and robust prognostic tool where the type of multiple sclerosis and the progression profile can be predicted and guide the choice of disease modifying therapy before irreversible clinical deficit accumulation manifests (Alastair Compston Ian McDonald John Noseworthy Hans Lassmann David Miller Kenneth Smith Hartmut Wekerle Christian Confavreux, 2005; Axtell et al., 2010).

MagLev is already known to be a low-cost separation technique based on matter density that takes advantage of gravitational and magnetic forces acting on diamagnetic particles suspended in a paramagnetic liquid medium. Recent developments in MagLev technologies have yielded new applications in biomedical engineering including cell separation and density analysis of biosystems (Ashkarran et al., 2020a; Ge et al., 2020, 2017; Hennek et al., 2015; Ilievski et al., 2011; Lockett et al., 2013; Mirica et al., 2011, 2010; Nemiroski et al., 2016; Subramaniam et al., 2014). Our recent case studies (Ashkarran et al., 2020a, 2020c, 2020b) showed that MagLev optic images of levitated proteins, subjected to machine-learning analysis, could offer valuable information on the individual's health status (Ashkarran et al., 2020b) and serve as "fingerprints", to discriminate between healthy and opioid use disorder (OUD) individuals (Ashkarran et al., 2020c). However, potential error sources encountered from practical applications of the method, e.g., errors in the biological preprocessing steps and/or during camera recordings, have not been addressed in the previous studies. Additionally, the analysis of MagLev images so far has been solely based on binary data cases (Ashkarran et al., 2020b).

To fill these gaps, here in this study, we aim to develop a MagLev-based robust predictive analytics framework that can not only diagnose MS from healthy controls but also classify them based on their types. Our findings revealed that levitating plasma proteins result in the formation of ellipsoidal patterns over time upon injection into the MagLev system containing superparamagnetic solution. This serves as a proof-of-concept study into the utility of this technique in the clinical setting.

2. Overall framework

Fig. 1 summarizes the steps in this study schematically. **Fig. 1a-c** shows the experimental setup (see Methods) and **Fig. 1d** illustrates the proposed modeling framework. Initially, normalized intensity histograms of MagLev images are derived to provide low-dimensional fingerprints of plasma samples. Next, the desired levitation time-frame in the process of MagLev is identified by a statistical distance technique. Finally, once the outlier MagLev images are identified and removed, a learning model is developed to classify the type of MS. The modeling framework was developed and trained using Python 3.7, OpenCV 4.2.0 (https://opencv.org/) and scikit-learn 0.24.1 (https://scikit-learn.org/) on a PC with Intel Core i7-8700 CPU 3.6 GHz, and 32G RAM.

Preprints (www.preprints.org) | NOT PEER-REVIEWED | Posted: 10 November 2022 doi:10.20944/preprints202211.0187.v1

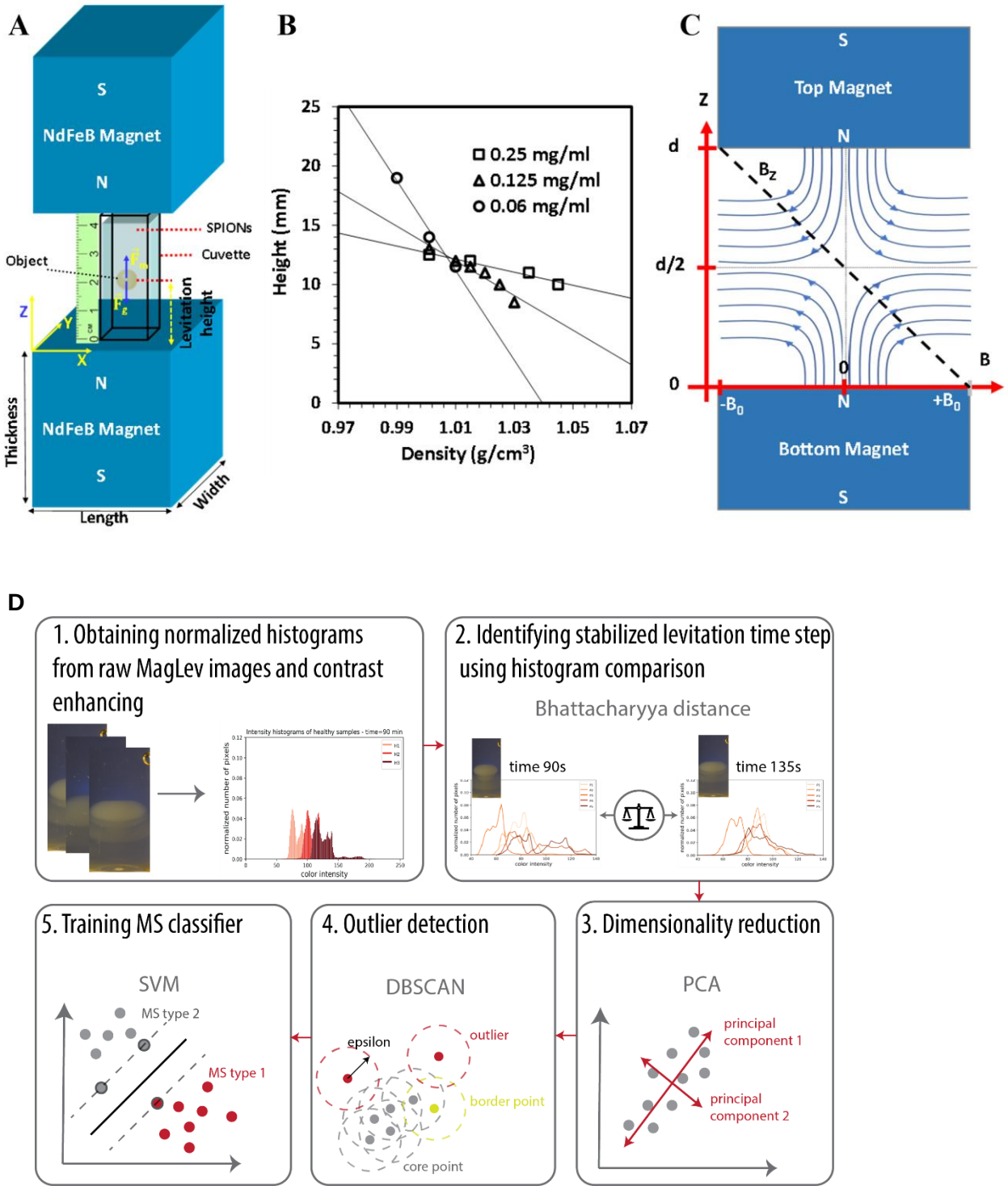

Figure 1. Representation of MagLev system configuration and proposed ML-based framework for detecting MS types. (A) Schematic showing the configuration of representative MagLev system. **(B)** Calibration curves of the MagLev system showing the linear relation between density of standard density glass beads and their corresponding levitation heights at different concentrations of SPIONs. **(C)** The pattern of the magnetic field lines between the magnets with like poles facing each other. **(D)** An overview of the detail of the proposed analysis pipeline.

The optical images of healthy individuals (n=2) as control and various MS patients (PPMS: n=3, RRMS: n=14, SPMS: n=5) were collected using the MagLev system (see **Fig. 2** for levitation patterns of various types of MS plasma proteins over the time, as

Preprints (www.preprints.org) | NOT PEER-REVIEWED | Posted: 10 November 2022 doi:10.20944/preprints202211.0187.v1

representatives). No sample related to PRMS was available in our collected clinical dataset. In each experiment, 36 images were captured every 5 minutes (total levitation time=180 minutes). All stored images were then cropped into the same region of interest to obtain the normalized intensity histogram of each image (**Fig. 1d, part 1)**. **Fig. 3** shows the histogram of a representative image obtained from MagLev system. The red curves in this figure are the cumulative distribution functions (CDF) of histograms. Two peaks appearing on this histogram represent plasma content and dark background. The horizontal axis shows 256 total variations and the vertical axis represents the normalized number of pixels in each greyscale tone. The stretched normalized histogram for the representative image (namely using a percentile stretching by clipping 2% of the data from both ends) is presented in **Fig. 3b**. As can be inferred by comparing the MagLev images in **Fig. 3**, the contrast stretching has enhanced the visual differentiation of features in the original image. The sharp rise in **Fig. 3a** is moderated by contrast stretching in **Fig. 3b** which stretches the horizontal axis and yields more distinct peaks.

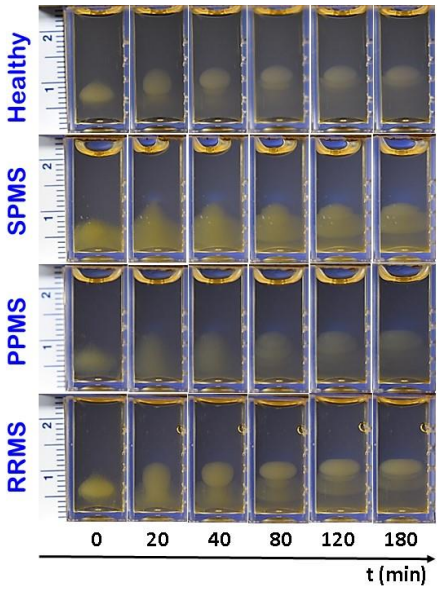

Figure 2. Photographs of the levitation patterns of plasma protein samples over time. Formation of various ellipsoidal patterns over the time upon injection of three types of various MS and healthy individual human plasma proteins into the MagLev system.

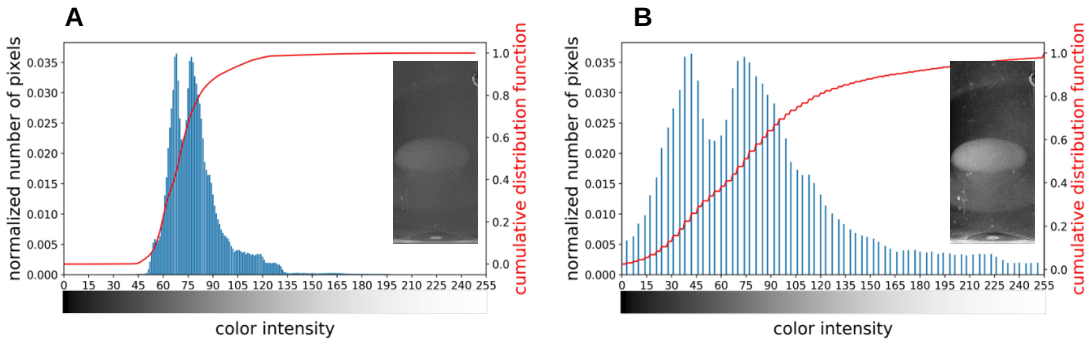

Figure 3. Effect of contrast stretching on MagLev images. (A) Representative normalized (relative to the total number of pixels in each image) intensity histogram of a MagLev image. The very low intensity peaks (black regions) correspond to no-protein content, whereas higher color intensities correspond to the protein content regions. (B) The stretched normalized histogram (normalization is done after contrast stretching) within 2nd and 98th percentiles. Comparing the cumulative distribution of bins in the histograms (shown as red curve), notice how the stretching transforms the abrupt change in the original histogram to a more gradual variation with more distinct peak, which can be particularly useful for outlier detection.

 doi:10.20944/preprints202211.0187.v1

As the levitation proceeds, the samples tend to preserve their shapes, especially when reaching the final stages of the levitation process (**Fig. 2**). Studying not-fully shaped (stabilized) layers' profiles can lead to an immature inference about the data and not suitable for reliable machine learning. Thus, deciding which time step should be selected for further analysis is vital. In other words, given each type of disease, a preprocessing pipeline needs to be designed for MagLev in order to detect the time step at which the samples physically reach to an equilibrium, and their geometrical features are statistically stabilized (**Fig. 1d, part 2**). To do so, at each time step, the grayscale histograms of each sample over time were compared with their preceding image using Bhattacharyya distance (BD) (Derpanis, 2008). A decrease in the value of the distance metric suggests that the sample is reaching to its stable profile.

The normalized histograms derived from the raw images were 255-dimensional vectors. Considering the limited number of available samples, the complex and high-dimensional feature space resulted from the histograms can drastically decline the performance of the ML models (i.e., the curse of dimensionality). Once the optimum time step is determined, the dimensions of the corresponding normalized images are reduced by implementing Principal Component Analysis (PCA) (Jolliffe and Cadima, 2016) (**Fig. 1d, part 3**).

In practice, the images captured from the plasma samples are uncontrollably subjected to different sources of noise and errors, such as those in the biological preprocessing steps and/or during camera recordings. Such outliers can have destructive effects on the performance of the predictive models as they convey faulty information which is not representative of the real data distribution(Hodge and Austin, 2004). Here, the Density-Based Spatial Clustering of Applications with Noise (DBSCAN) (Emadi and Mazinani, 2018), a hierarchical clustering algorithm, was employed as a data preprocessing step to detect and remove potential image outliers (**Fig. 1d, part 4**).

Once the outliers are detected and removed, the preprocessed data is used to train a supervised classification model, namely, Support Vector Machines (SVM) (Vapnik et al., 1997). In order to investigate the effect of the nonlinear behavior in the MS dataset on the performance of the learning models, two kernel functions, namely, Radius Basis Function (RBF) and Linear, were selected in the SVM model (**Fig. 1d, part 5**).

3. Materials and methods

3.1. Experimental setup

A 30 mg/ml superparamagnetic solution (SPIONs, purchased from Feraheme, www.feraheme.com) was used as a MagLev medium and diluted with phosphate buffered saline (PBS 1X, HyClone) solution to 0.06 mg/ml for all experiments. Plasma from healthy individuals and MS patients was provided through our collaboration with the Multiple Sclerosis Center at the University of Massachusetts Medical Center, Worcester, MA. For all experiments 100 µl of as received human plasma proteins with different types of MS diseases, was spiked into the plastic cuvette containing SPIONs solution, placed into the MagLev system and levitated for 3 hours until they reached their equilibrium positions within the MagLev system. It is noteworthy that after 3 hours no changes in levitation pattern of protein samples were observed. Fluorescent polyethylene microparticles (www.cospheric.com) with known densities and standard density solid glass particles (www.americandensitymaterials.com) were used for calibration of the MagLev system (**Fig. 1b and S3** of Supplementary Information (SI)). All conventional MagLev systems have a pair of similar permanent magnets with similar poles face to face and a separation distance of d. We have used a standard MagLev platform using two blocks of N42-grade neodymium (NdFeB) cubic magnets (25.4 mm length, 25.4 mm width, and 50.8 mm height) and a separation distance of 25 mm in the present work, which is depicted in **Fig. 1a**. Disposable plastic cuvettes were cut to fit exactly between two magnets to serve as a levitation container. The principles of the MagLev technique and details of the underlying equations are reported by others and our group (Ashkarran et al., 2020c, 2020a; Ge et al., 2020; Nemiroski et al., 2016). Two blocks of cubic-shape NdFeB permanent magnets

Preprints (www.preprints.org) | NOT PEER-REVIEWED | Posted: 10 November 2022 doi:10.20944/preprints202211.0187.v1

(grade N42, Model # NB044) were provided from magnet4less (**Fig. 1b**). Levitation profiles of the particles were recorded by a Nikon D750 digital camera containing a 105 mm Nikkor Microlense and a millimeter scale ruler. A gauss meter (vector/magnitude Gauss meter model VGM, Alphalab), was used to measure the magnetic field strength between the magnets (~ 0.5 T on both magnet's surfaces).

3.2. Data preparation and analysis pipeline

3.2.1. Sampling and image processing

The histograms represent the distribution of tonal variations in images. The peaks and valleys appearing on the histograms provide useful information about the different phases in each image and the phases can be separated by thresholding (Solomon and Breckon, 2011). Despite their simple implementation, histograms are frequently used for addressing complex problems such as over/under exposure, brightness and contrast in image processing methods. In addition, they are effective tools for edge detection, image segmentation and classification; for example, brain tumor detection with histogram equalization (Ulku and Camurcu, 2013). The normalization at this step is calculated based on the relative values of the vertical axis to the total number of pixels in each image. In other words, it changes the range of the vertical axis in the histogram, to be consistent among all images. There is another type of normalization in image processing known as 'contrast stretching' (Solomon and Breckon, 2011), that stretches the range of pixel intensity values (horizontal axis) to fill the entire dynamic range. Contrast stretching is usually implemented for improving quality of blurry images (or when the phases in an image are very close to each other in terms of greyscale tone).

3.2.2. Identification of a stabilized time-frame from MagLev recordings

More specifically, the Bhattacharyya distance (BD), which measures the dissimilarity of two histograms using the Bhattacharyya coefficient – a divergence-type metric between two distributions – was employed (Derpanis, 2008). Given two probability distributions, p and q over the same domain X, the BD, which can take a value from 0 to 1, is defined as:

$$d(p,q) = \sqrt{1-\rho(p,q)} \tag{1}$$

where ρ is the Bhattacharyya coefficient:

$$\rho(p,q) = \sum_x^N \sqrt{1-p(x)q(x)} \tag{2}$$

and x is a class drawn from the domain x.

3.2.3. Dimensionality reduction

A common and powerful practice to tackle the dimensionality of the input spaces is PCA. This tool converts a set of correlated variables into a set of uncorrelated ones using an orthogonal transformation while preserving data variability to the greatest extend possible. While the first principal component (PC1) projects the observations onto the direction with the largest variance, the second principal component (PC2) is fully uncorrelated with the first one and has the second-largest variance; and accordingly, other principal components can be defined. Since the new variables (PCs) better describe the overall variance in the dataset, by plotting the principal components, distinct clusters of samples may appear.

3.2.4. Outlier detection using unsupervised machine learning

Clustering, as an unsupervised machine learning method, separates and groups the samples based on their similarities and differences in the feature space. The DBSCAN is a powerful clustering method widely used in a variety of applications (Emadi and Mazinani, 2018). It has been shown that DBSCAN is able to successfully detect both

Preprints (www.preprints.org) | NOT PEER-REVIEWED | Posted: 10 November 2022 doi:10.20944/preprints202211.0187.v1

clusters and noise (outliers) while maintaining a robust performance in the presence of limited data (Schubert et al., 2017). Unlike partitioning clustering algorithms (e.g., k-means), the hierarchical algorithms do not require the number of clusters to be specified beforehand and they are able to capture complex cluster shapes (e.g., non-convex) (Ester et al., 1996). Particularly, in DBSCAN, a cluster forms when within a neighborhood of a given radius for a point (called ϵ-neighborhood), there is at least a preset minimum number of points (called $MinPts$). Additionally, a point belongs to a cluster whether it has $MinPts$ within its ϵ-neighborhood (core point) or it is located in the ϵ-neighborhood of a core point (border point). Once a cluster is initiated, it can grow if the neighbor points satisfy the density requirements of either core or border points. Finally, in a DBSCAN model, an outlier (noise) is defined as the point that does not belong to any identified cluster (Ester et al., 1996). The performance of DBSCAN is governed by its above described two parameters ($MinPts$ and ϵ) and identifying their appropriate values (given an application) is crucial for obtaining a useful modeling outcome. Hypothetically, finding optima of these parameters requires knowledge about every cluster existing in the dataset. As such information is often lacking in practice (e.g., the number of clusters is not known as in unsupervised setting; or when the sample size within each cluster is small), empirical approaches need to be implemented. Some heuristic methods have been proposed in the literature which provide an estimate of the optimal parameters setting for DBSCAN. Birant and Kut (Birant and Kut, 2007) has proposed an equation which estimates the $MinPts$ as a function of sample size:

$$MinPts = \ln(N) \tag{3}$$

where N is the total number of data points. In the same direction, as elaborated in the original DBSCAN paper (Ester et al., 1996), the proper value for ϵ can be approximated by plotting the *sorted k-dist* graph. The point in the graph on which the "plain" area is transformed into a "valley" (called "elbow" region) is mapped to the y-axis (k-distance) to find an estimate of optimal ϵ.

3.2.5. Supervised classification model for MS data

Introduced by Vapnik (Vapnik et al., 1997), SVM is known as a powerful and versatile supervised learning algorithm, which has been successfully utilized in a wide range of applications (Meng et al., 2019; Pławiak et al., 2019). SVM exhibits a robust performance against nonlinear datasets, as it employs kernel functions to simplify the feature space by mapping the complex input data to a high-dimensional space. In turn, it transforms the nonlinear structure of the data into linearly separable classes. The classification decision boundary in the SVM is defined by maximizing its distance from the edge instances (closest instances to the decision boundary) of each class (i.e., minimizing the structural risk) (Vapnik et al., 1997). RBF uses similarity features to generate the high-dimensional space, making it a suitable choice when the relation between the input variables and class labels is nonlinear (e.g., MS dataset). The RBF kernel is defined as:

$$K(x, x_j) = \exp(-\gamma \|x - x_j\|^2) \tag{4}$$

where γ (inverse of the RBF kernel standard deviation) indicates how far the effect of each point reaches for measuring similarity features.

4. Results

4.1. Levitated plasma proteins of MS patients in MagLev system

To levitate human plasma proteins in our MagLev system, we have used a suspension of SPIONs for the MagLev medium. Toxicity of conventional paramagnetic solutions (e.g., $GdCl_3$ and gadobutrol) particularly at high concentrations (i.e., ~ 100 mM and higher) prevents the use of common paramagnetic liquids as MagLev medium for most biological

 doi:10.20944/preprints202211.0187.v1

applications. We have previously shown that the plasma proteins denature and sediment in the conventional paramagnetic liquids due to interactions with the high concentration of gadolinium complex ions (Ashkarran et al., 2020c). To solve the biocompatibility issue of the most common MagLev media, we introduced ferumoxytol (an FDA-approved superparamagnetic liquid) as a new biocompatible MagLev medium for levitation of human plasma proteins. Superparamagnetic solutions not only are biocompatible with human plasma proteins but also provide a larger magnetic susceptibility as a MagLev medium compared to common paramagnetic liquids, and therefore, a significantly faster separation of protein molecules in solution (Kandasamy and Maity, 2015; Li et al., 2017). Consequently, the exposure time of the levitating biomolecules to the MagLev medium will be significantly reduced which is a great advantage for most biomedical applications and diagnostic purposes. **Fig. 2** shows levitation profiles of human plasma proteins of various healthy individuals and MS patients containing three different types of MS as representatives (optical images of the levitation patterns of representative MS plasma proteins in the MagLev system are presented in **Fig. S1-S3** of SI). The plasma proteins created ellipsoidal patterns within the MagLev system during the levitation process. Formation of ellipsoidal patterns starts in a few minutes and changes in pronounced patterns over three hours (see for examples plasma patterns and their appearance differences at 20 and 120 minutes in **Fig. 2** and **Fig. S2-S4** of SI). We tested 24 human plasma samples from male and female individuals with various ethnicities and ages who were diagnosed with RR, PP, or SP MS and monitored their corresponding levitation patterns. We observed a distinct pattern in all levitated MS human plasma proteins as compared to healthy plasma. The observed patterns from levitated plasma proteins were highly reproducible, as all experiments were repeated at least three times and yielded identical patterns.

4.2. Identification of stabilized time-frames of MagLev images

Optical images of levitated plasma proteins of healthy and MS patient plasma donors were extracted from the MagLev system and used to develop a classification prediction model to determine whether the appeared plasma patterns in the MagLev system can provide "fingerprints" which can be processed with machine learning to differentiate between healthy individuals and MS patients as well as differentiate MS subtypes. Finding a stabilized time-frame using levitation profiles of plasma proteins in the MagLev system, is one of the crucial parameters which affect the data processing and the selection of inappropriate time-frames can cause unreliable machine learning analysis. The histograms comparison was performed using the OpenCV python library. As illustrated in **Fig. 4b**, on average, the Bhattacharyya distance (BD) is at its lowest value (<0.2; i.e., an 80% relative match between two subsequent histograms) when comparing time-steps 135 min and 180 min, suggesting that the samples have been fairly stabilized at levitation time of 135 min. This could also be confirmed by visually comparing the images in **Fig. 4a** in which time-steps 135 min and 180 min exhibit very similar profiles (see also **Fig. S2-S4** for the progress of levitation patterns of various plasma proteins). Additionally, two other distance metrics, namely, chi-square distance and Pearson's correlation, were employed and both verified the results attained by the BD analysis (see **Fig. S5** and **Fig. S6** of SI) [11]. Therefore, the levitation pattern of all samples at t=135 min was selected for all further statistical analysis and modeling.

Preprints (www.preprints.org) | NOT PEER-REVIEWED | Posted: 10 November 2022 doi:10.20944/preprints202211.0187.v1

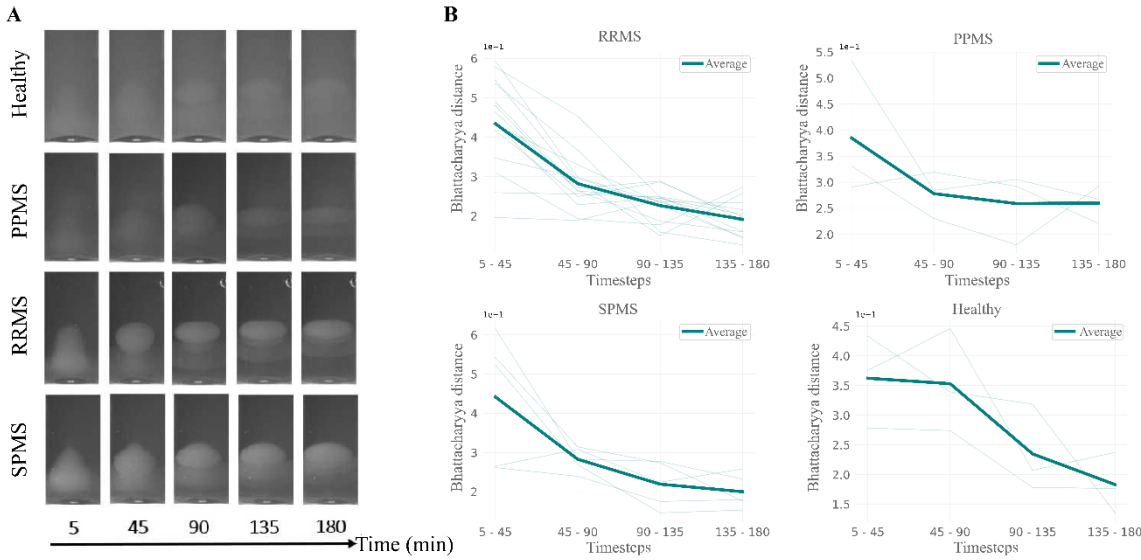

Figure 4. BD calculates the MagLev images similarities over time as a measure for identifying the stabilization time. (A) Greyscale images of selected samples of each group (healthy, PPMS, RRMS and SPMS) over the time. **(B)** Variation of the BD of MagLev images at different time steps (5-45-90-135-180 min) with respect to previous timestep. For both control and MS groups, timesteps 135 and 180 exhibit highest similarities (lowest distances) suggesting that samples reach to a stable state at t=135 min.

4.3. PCA and Dissimilarity Analysis

PCA plot of the histograms of MagLev images after outlier removal is shown in **Fig. 5a** and results demonstrated two disguisable clusters between the healthy group and MS sub-groups. Pairwise PERMANOVA test also confirms this conclusion with the most significant difference being between healthy and RRMS groups (p-value of 0.021). This difference results from the far distance between the peaks in average intensity histograms of healthy and MS groups illustrated in **Fig. 5b**.

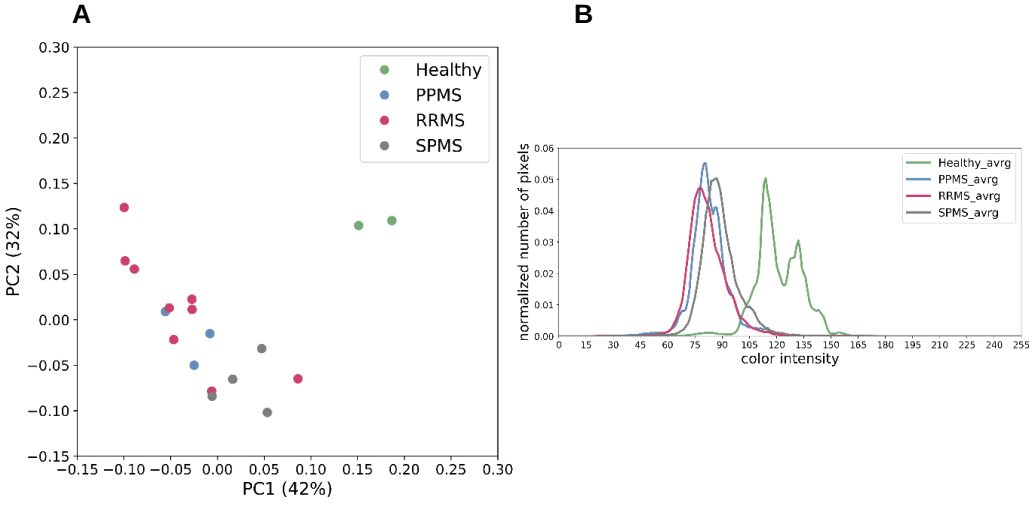

Figure 5. Reduced-order representation of different groups of samples. (A) PCA score plot after automated outlier detection at t=135 min. The retained variance by the two principal components is about 75%. **(B)** Average intensity histograms of each group of healthy, PPMS, RRMS, and SPMS at t=135 min, showing differences between the groups.

4.4. Outlier detection

Preprints (www.preprints.org) | NOT PEER-REVIEWED | Posted: 10 November 2022 doi:10.20944/preprints202211.0187.v1

Considering the number of samples used in this study, we applied the DBSCAN separately to the classes with at least four samples; namely, RRMS and SPMS. The $MinPts$ for the RRMS dataset was calculated as: $ln(13) = 2.56$. Therefore, DBSCAN was performed with $MinPts \in \{2,3\}$. Additionally, the sorted k-distance graph was plotted for different values of k (including the values of $MinPts$ found above) to determine ϵ. As illustrated in **Fig. 6a**, for all values of k, the elbow region collectively appeared in the same spot (shown by the dashed circle) and thereby the optimal value of ϵ could be approximated as 0.045. DBSCAN analysis resulted in a cluster of normal images at the center and corrupted samples (distanced from the main cluster) as outliers (**Fig. 6b**), similarly when using $MinPts$ 2 or 3. A visual comparison of MagLev images also confirmed that DBSCAN was able to successfully distinguish the faulty images from normal samples (see **Fig. S7** of **SI**). Subsequently, detected outliers were removed from the rest of the analysis.

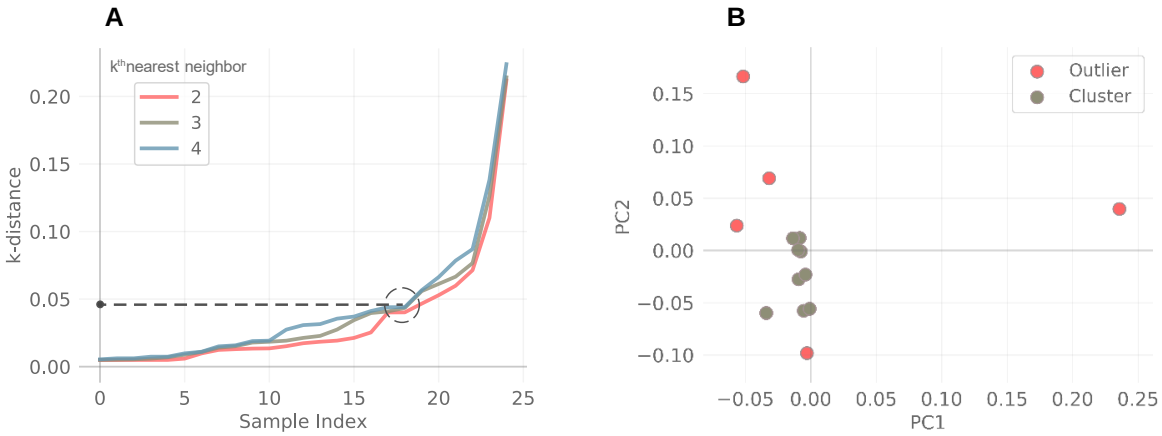

Figure 6. Graphs showing the DBSCAN's hyperparameter tuning and outlier detection on MagLev samples. (A) Identifying the optimal ϵ hyperparameter in DBSCAN using the K-distance plot. The figure shows the distance for three different values for the kth nearest neighbors (2, 3 and 4). The optimal ϵ value corresponds to the sudden shift in the curve slope (called 'elbow region', shown by the dashed circle). **(B)** Example of automated outlier detection for RRMS data using DBSCAN method.

4.5. SVM classification model

The hyperparameters of the SVM model, namely $\boldsymbol{C}$ (controlling the soft margins in the cost function) and $\boldsymbol{\gamma}$ (only used for RBF kernel), were selected using a grid search algorithm followed by cross-validation. The hyper-parameters were tuned by optimizing the F1-score over Leave-One-Out cross-validation and set to $\boldsymbol{C = 1000}$ and $\boldsymbol{\gamma = 3}$ for RBF kernel SVM and $\boldsymbol{C = 100}$ for linear SVM. Receiver Operating Characteristic (ROC) curves (**Fig. 7a**) suggested that the RBF kernel SVM (with the Area Under Curve (AUC)=0.77 and F1 score=71%) exhibits a noticeably better classification performance than the linear SVM (AUC=0.52 and F1 score=44%). **Fig. 7b** illustrates the class regions via decision boundaries predicted by the RBF kernel SVM. For comparing the classes statistically, pairwise PERMANOVA was then performed among MS groups. The result shows a significant distinction between PPMS-SPMS and RRMS-SPMS with p-values of 0.031 and 0.033, respectively. However, RRMS and PPMS observations were not found significantly different. It can also be inferred from Figure 5a that the centers of these two groups are very close. Hypothetically, this could be because small N and clinically, RRMS has a wide range of disease diversity (Figure 5a) depending on age, medical history of patients, etc. which would make its exact identification fuzzy.

Preprints (www.preprints.org) | NOT PEER-REVIEWED | Posted: 10 November 2022 doi:10.20944/preprints202211.0187.v1

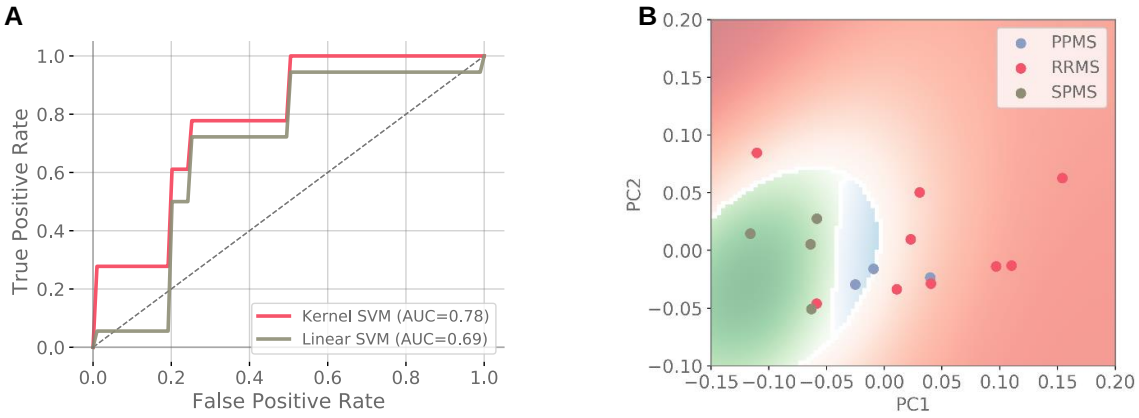

Figure 7. Generalization performance of linear and kernel SVM trained on limited MagLev images of MS samples. (A) ROC of linear SVM and kernel (RBF) SVM models. SVM with RBF transformation demonstrates a better overall performance (higher area under curve). (B) The produced classified feature space by the kernel SVM prediction model. In contrast to linear SVM, the kernel SVM allows non-linear decision boundaries. Darker (lighter) regions in each class corresponds to the higher (lower) prediction scores (higher (lower) classification confidence).

5. Conclusions

We demonstrated a proof-of-concept study that the combination of optical images of levitation plasma proteins and machine learning technique enables us to classify three types of MS: RRMS, SPMS, and PPMS. Particularly, using the developed expert system, we were able to enhance (based on histogram normalization and contrast stretching) the MagLev images, detect and remove the outlier images, and classify the different types of MS disease. The current preliminary results showed that even with a small clinical dataset available, a fair prediction model can be achieved with an F1 score of 71% and this should be improved as the sample size become larger. Using omic technologies, it will vbe valuable to identify specific biomarkers that can differentiate MS subtypes and lack of such analyses are part of study limitations. However, one can hypothesize that magLev technique is more sensitive at distinguishing MS subtypes than conventional plasma protein measurements, and we hypothesize this difference in sensitivity is dependent upon taking all of the charges and composition of the blood plasma into account for differentiations of MS subtypes, rather than a curated set of biomarkers. Also, this should be noted that futrtehr works are needed to investigate wheather any other disease can lead to similar plasma image structures or not. For these, the presented preliminary framework herein may not be used as a full screening tool for the population level, as more plasma samples and system optimization are required. Regardless, the proposed analysis and data processing framework remains a valuable future application of MagLev for MS and other diagnosis purposes.

Data availability: All relevant data are available from the authors.

Competing interests: MM discloses that i) he is a co-founder and director of the Academic Parity Movement, a non-profit organization dedicated to addressing academic discrimination, violence and incivility; and ii) he receives royalties/honoraria for his published books, plenary lectures, and licensed patent.

Abbreviations: DBSCAN = Density-Based Spatial Clustering of Applications; MagLev = magnetic levitation; MS = multiple sclerosis; PCA = Principal Component Analysis; PPMS = primary-progressive MS; PRMS = progressive-relapsing MS; RBF = Radius Basis Function; RRMS = Relapsing-Remitting; SPMS = secondary-progressive MS; SVM = Support Vector Machines.

References

1.Alastair Compston Ian McDonald John Noseworthy Hans Lassmann David Miller Kenneth Smith Hartmut Wekerle Christian Confavreux, 2005. McAlpine's Multiple Sclerosis, 4th editio. ed. Churchill Livingstone, London.

2.Ashkarran, A.A., Dararatana, N., Crespy, D., Caracciolo, G., Mahmoudi, M., 2020a. Mapping the heterogeneity of protein corona by ex vivo magnetic levitation. Nanoscale 12, 2374–2383.

3.Ashkarran, A.A., Olfatbakhsh, T., Ramezankhani, M., Crist, R.C., Berrettini, W.H., Milani, A.S., Pakpour, S., Mahmoudi, M., 2020b. Evolving magnetically levitated plasma proteins detects opioid use disorder as a model disease. Adv. Healthc. Mater. 9, 1901608.

4.Ashkarran, A.A., Suslick, K.S., Mahmoudi, M., 2020c. Magnetically levitated plasma proteins. Anal. Chem. 92, 1663–1668.

5.Axtell, R.C., De Jong, B.A., Boniface, K., Van Der Voort, L.F., Bhat, R., De Sarno, P., Naves, R., Han, M., Zhong, F., Castellanos, J.G., Mair, R., Christakos, A., Kolkowitz, I., Katz, L., Killestein, J., Polman, C.H., De Waal Malefyt, R., Steinman, L., Raman, C., 2010. T helper type 1 and 17 cells determine efficacy of interferon-B in multiple sclerosis and experimental encephalomyelitis. Nat. Med. 16, 406–412. https://doi.org/10.1038/nm.2110

6.Birant, D., Kut, A., 2007. ST-DBSCAN: An algorithm for clustering spatial–temporal data. Data Knowl. Eng. 60, 208–221.

7.Derpanis, K.G., 2008. The bhattacharyya measure. Mendeley Comput. 1, 1990–1992.

8.Emadi, H.S., Mazinani, S.M., 2018. A novel anomaly detection algorithm using DBSCAN and SVM in wireless sensor networks. Wirel. Pers. Commun. 98, 2025–2035.

9.Ester, M., Kriegel, H.-P., Sander, J., Xu, X., 1996. A density-based algorithm for discovering clusters in large spatial databases with noise., in: Kdd. pp. 226–231.

10.Ge, S., Nemiroski, A., Mirica, K.A., Mace, C.R., Hennek, J.W., Kumar, A.A., Whitesides, G.M., 2020. Magnetic Levitation in Chemistry, Materials Science, and Biochemistry. Angew. Chemie Int. Ed. 59, 17810–17855. https://doi.org/10.1002/anie.201903391

11.Ge, S., Semenov, S.N., Nagarkar, A.A., Milette, J., Christodouleas, D.C., Yuan, L., Whitesides, G.M., 2017. Magnetic Levitation to Characterize the Kinetics of Free-Radical Polymerization. J. Am. Chem. Soc. 139, 18688–18697. https://doi.org/10.1021/jacs.7b10901

12.Hauser, S.L., Cree, B.A.C., 2020. Treatment of Multiple Sclerosis: A Review. Am. J. Med. 133. https://doi.org/10.1016/j.amjmed.2020.05.049

13.Hennek, J.W., Nemiroski, A., Subramaniam, A.B., Bwambok, D.K., Yang, D., Harburg, D. V., Tricard, S., Ellerbee, A.K., Whitesides, G.M., 2015. Using Magnetic Levitation for Non-Destructive Quality Control of Plastic Parts. Adv. Mater. 27, 1587–1592. https://doi.org/10.1002/adma.201405207

14.Hodge, V., Austin, J., 2004. A survey of outlier detection methodologies. Artif. Intell. Rev. 22, 85–126.

15.Ilievski, F., Mirica, K.A., Ellerbee, A.K., Whitesides, G.M., 2011. Templated self-assembly in three dimensions using magnetic levitation. Soft Matter 7, 9113–9118. https://doi.org/10.1039/c1sm05962a

16.Jolliffe, I.T., Cadima, J., 2016. Principal component analysis: a review and recent developments. Philos. Trans. R. Soc. A Math. Phys. Eng. Sci. 374, 20150202.

17.Kandasamy, G., Maity, D., 2015. Recent advances in superparamagnetic iron oxide nanoparticles (SPIONs) for in vitro and in vivo cancer nanotheranostics. Int. J. Pharm. https://doi.org/10.1016/j.ijpharm.2015.10.058

18.Li, K., Nejadnik, H., Daldrup-Link, H.E., 2017. Next-generation superparamagnetic iron oxide nanoparticles for cancer theranostics. Drug Discov. Today. https://doi.org/10.1016/j.drudis.2017.04.008

19.Lockett, M.R., Mirica, K.A., Mace, C.R., Blackledge, R.D., Whitesides, G.M., 2013. Analyzing Forensic Evidence Based on Density with Magnetic Levitation. J. Forensic Sci. 58, 40–45. https://doi.org/10.1111/j.1556-4029.2012.02221.x

20.Lublin, F.D., 2014. New Multiple Sclerosis Phenotypic Classification. Eur. Neurol. 72, 1–5. https://doi.org/10.1159/000367614

21.Meng, E., Huang, S., Huang, Q., Fang, W., Wu, L., Wang, L., 2019. A robust method for non-stationary streamflow prediction based on improved EMD-SVM model. J. Hydrol. 568, 462–478.

22.Mirica, K.A., Ilievski, F., Ellerbee, A.K., Shevkoplyas, S.S., Whitesides, G.M., 2011. Using magnetic levitation for three dimensional self-assembly. Adv. Mater. 23, 4134–4140. https://doi.org/10.1002/adma.201101917

23.Mirica, K.A., Phillips, S.T., MacE, C.R., Whitesides, G.M., 2010. Magnetic levitation in the analysis of foods and water. J. Agric. Food Chem. 58, 6565–6569. https://doi.org/10.1021/jf100377n

24.Nelson, L.M., Wallin, M.T., Marrie, R.A., Culpepper, W.J., Langer-Gould, A., Campbell, J., Buka, S., Tremlett, H., Cutter, G., Kaye, W., Wagner, L., Larocca, N.G., 2019. A new way to estimate neurologic disease prevalence in the United States: Illustrated with MS. Neurology 92, 469–480. https://doi.org/10.1212/WNL.0000000000007044

25.Nemiroski, A., Kumar, A.A., Soh, S., Harburg, D. V., Yu, H.D., Whitesides, G.M., 2016. High-Sensitivity Measurement of Density by Magnetic Levitation. Anal. Chem. 88, 2666–2674. https://doi.org/10.1021/acs.analchem.5b03918

26.Pławiak, P., Abdar, M., Acharya, U.R., 2019. Application of new deep genetic cascade ensemble of SVM classifiers to predict the Australian credit scoring. Appl. Soft Comput. 84, 105740.

27.Reich, D.S., Lucchinetti, C.F., Calabresi, P.A., 2018. Multiple Sclerosis. N. Engl. J. Med. 378, 169–180. https://doi.org/10.1056/NEJMra1401483

28.Schubert, E., Sander, J., Ester, M., Kriegel, H.P., Xu, X., 2017. DBSCAN revisited, revisited: why and how you should (still) use DBSCAN. ACM Trans. Database Syst. 42, 1–21.

29.Solomon, C., Breckon, T., 2011. Fundamentals of Digital Image Processing: A practical approach with examples in Matlab. John Wiley & Sons.

 doi:10.20944/preprints202211.0187.v1

30. Subramaniam, A.B., Yang, D., Yu, H.D., Nemiroski, A., Tricard, S., Ellerbee, A.K., Soh, S., Whitesides, G.M., 2014. Noncontact orientation of objects in three-dimensional space using magnetic levitation. Proc. Natl. Acad. Sci. U. S. A. 111, 12980–12985. https://doi.org/10.1073/pnas.1408705111
31. Ulku, E.E., Camurcu, A.Y., 2013. Computer aided brain tumor detection with histogram equalization and morphological image processing techniques, in: 2013 International Conference on Electronics, Computer and Computation (ICECCO). IEEE, pp. 48–51.
32. Vapnik, V., Golowich, S.E., Smola, A.J., 1997. Support vector method for function approximation, regression estimation and signal processing, in: Advances in Neural Information Processing Systems. pp. 281–287.
33. Wallin, M.T., Culpepper, W.J., Campbell, J.D., Nelson, L.M., Langer-Gould, A., Marrie, R.A., Cutter, G.R., Kaye, W.E., Wagner, L., Tremlett, H., 2019. The prevalence of MS in the United States: a population-based estimate using health claims data. Neurology 92, e1029–e1040.